Analysis of variable angle tow composites structures using variable kinematic models

Analysis of variable angle tow composites structures using variable kinematic models

A. Viglietti[a,1], E. Zappino[a,2,*], E. Carrera[a,3]

[a] *Politecnico di Torino, Corso Duca degli Abruzzi 24, 10129 Torino, Italy*

Abstract

This work presents a refined beam model based on the Carrera Unified Formulation for the free-vibration analyses of variable stiffness composite laminate characterized by layers with curvilinear fibers. These models introduce a refined kinematic description over the cross-section to obtain a 3D displacement field. Taylor and Lagrange polynomials have been used to describe the cross-sectional variables that is, equivalent single layer and layer-wise approaches have been considered. Variable stiffness composite materials have been introduced considering a continuous variation of the lamination angle thanks to an ad hoc integration scheme. Extensive validation of the models has been performed including convergence analyses and comparisons with commercial codes. The results obtained using the present models have been compared with those from open literature considering composites with different values of thickness, lamination, and boundary conditions. The results show that the use of refined models is mandatory for the analysis of such structures where complex laminations may create strong mechanical couplings.

Keywords: CUF, VAT, VSCL, Variable Angle Tow, Variable Stiffness Composite Laminate, Beam model, Refined Model

*Corresponding author

Email addresses: andrea.viglietti@polito.it (A. Viglietti), enrico.zappino@polito.it (E. Zappino), erasmo.carrera@polito.it (E. Carrera)

[1] Research Assistant, Department of Mechanical and Aerospace Engineering.

[2] Assistant Professor, Department of Mechanical and Aerospace Engineering.

[3] Full Professor, Department of Mechanical and Aerospace Engineering.

1. Introduction

Composite materials are increasingly used in many engineering fields thanks to their lightness and the high mechanical performances. For this reason, many research activities are engaged to optimize traditional composite materials and to define modern advanced materials based on the fiber-reinforced laminate. Conventional composite materials consider a uniform lamination over the whole component (Constant Stiffness Composite Laminates - *CSCL*). High-performance structures, such as in the aerospace field, could be enhanced by the use of different lamination scheme in different areas, and for this reason, the Variable Stiffness Composite Laminates (*VSCL*) have been introduced. In order to modify the laminate stiffness locally, a possible method is the variation of the fiber volume fraction as presented in the work of Leisa and Martin [1] related to the control of the frequency values of a plate. Another simple approach to obtain panels with variable stiffness is represented by the variation of the number of the layers. Through the ply drop-off, an inner layer is terminated in order to vary the thickness and then the stiffness. Di Nardo and Lagace [2] studied the effects on the buckling and post-buckling behaviors of this kind of laminates. Modern composite manufactory technologies have led to a third method for the manufacturing of *VSCL*. New automatic processes have made possible the production of Variable Angle Tow (VAT) composites where the fibers are not constrained along a straight path but can follow curvilinear trajectories. A detailed overview of this process and other automated manufacturing methods can be found in the work by Dirk *et al.*[3]. This technology increases the design space and increases the freedom in the tailoring process to obtain the desired structural performances. VAT material capabilities can be exploited to control the stress fluxes, to increase the stiffness locally, to control the dynamic behavior of complex structures.

This idea was originally proposed by Hyer [4, 5] to overcome the discontinuities in the areas where the fiber orientation changes. The same author has shown in [6] how a curvilinear pattern of the fibers can be used to improve the buckling load in plates with the presence of holes. In the nineties, several researchers have investigated the characteristics of the *VSCL* in term of buckling and static deformation as shown in the works by Waldhart[7] or Langley[8]. Tatting, after a work on the variable stiffness composite cylinders [9], has proposed with Gurdal a design tool for the *VSCL* [10]. Lopes *et al.* [11] have presented how the curvilinear fibers can redirect the load fluxes from a central region to a stiffer area in order to improve the buckling stiffness. VAT materials have found a large application in the design of the aeroelastic response as shown in [12]. Weaver and

his collaborators have deeply investigated the buckling and post-buckling behavior of this class of composites [13, 14], studying also the optimization of VAT composite plates [15, 16]. Xiaodong *et al.* [17] investigates the buckling behavior of VAT plates affected by delamination areas. Ribeiro and Akhavan [18, 19] have used the First-Order Shear Deformation Theory (FSDT) for the evaluation of non-linear vibrations of VSCL plates. More recently, the same theory has been used in the work by Montemurro e Catapano [20], where is presented an optimization strategy for VAT laminates, and in the work by Zhou and Gosling [21] where they investigate the uncertainty of the mechanical performances of VAT plates. Ribeiro *et al.* [22] have exploited the accuracy of a Third Order Shear Theory to study the free vibration of thin and thick VSCL plates. The same authors have presented a work [23] in which a Layer-Wise (LW) theory and p-version finite element method have been used to evaluate the vibration modes of thin and thick variable stiffness plates. The same approach has also been used for geometrically non-linear static analyses [24]. The LW approach allows the accuracy to be increased thanks to the capability to describe aech layers separately. This topic is discussed in many works such as the manuscript by Robbin and Reddy [25] which propose a finite element (FE) model considering a LW displacement approximation, or the work by Shimpi and Ainapure [26] based on an FE beam model and a trigonometric LW shear deformation theory.

The present work proposes an extension of the Carrera Unified Formulation (CUF) to the analysis of variable angle tow structures. CUF has been developed for plate and shell by Carrera [27, 28] and then, extended for the beam case. When refined one-dimensional (1D) models are considered, the cross-sectional behavior is described through a function expansion. The CUF provides an efficient tool to derive refined models with any expansion order in a compact and unified manner. This approach produces accurate results for beams with arbitrary geometries like plate-shell ones [29]. In the CUF framework, two main classes of one-dimensional models have been developed: the Taylor models (TE), where the homonymous expansions are implemented [30, 31], and the Lagrange models (LE) that use the Lagrange polynomials [32]. The second approach led to a model where the unknowns are only the nodal displacements. Other models are those based on the Chebyshev Expansions [33] or the Hierarchical Legendre-type Expansions [34]. In this paper, for the first time, a formulation able to deal with VAT structures is introduced in the framework of the CUF. The aim of the work concerns the validation of the present model for free-vibration analyses on VAT structures and a critical analysis of the advantages of the refined models in the analysis of such structures. A first part is dedicated to a brief explanation of the theoretical model; an exhaustive

validation of the model is presented in the second part while the third section gives a comparison with the literature for thin and thick plates considering different boundary conditions. Finally, an accurate comparisons between LW and ESL models has been presented.

2. One-dimensional refined models

This section presents the theoretical model used in this work. A first part briefly introduces the CUF and the FEM solution adopted. A second part focuses on the implementation of the variable angle tow model.

2.1. Preliminaries

In the present model a beam can be generally oriented with respect to a global frame (x_g,y_g,z_g) and is described using a local frame (x,y,z) where y is the beam axis, and the plane $x-z$ defines the plane of the beam cross-section. Figure 1 shows these two frames considering a plate described through a beam model.

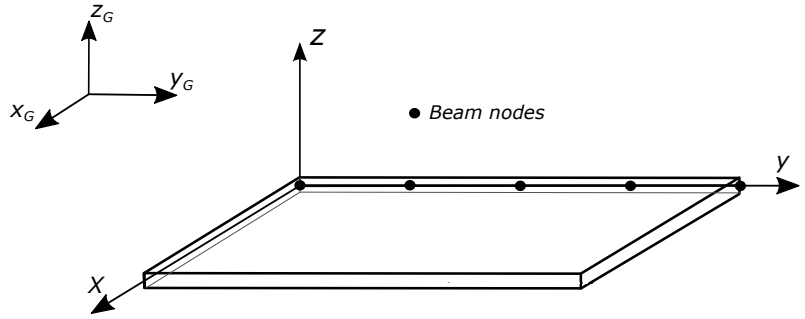

Figure 1: Global and local frames.

The local displacement vector can be written as:

$$\boldsymbol{u}(x,y,z) = \{u_x\, u_y\, u_z\}^T \tag{1}$$

The stress vector $\boldsymbol{\sigma}$ and the strain one $\boldsymbol{\epsilon}$ are defined using the following form:

$$\boldsymbol{\sigma}(x,y,z) = \{\sigma_{xx}, \sigma_{yy}, \sigma_{zz}, \tau_{xy}, \tau_{xz}, \tau_{yz}\}^T \tag{2}$$

$$\boldsymbol{\epsilon}(x, y, z) = \{\epsilon_{xx}, \epsilon_{yy}, \epsilon_{zz}, \epsilon_{xy}, \epsilon_{xz}, \epsilon_{yz}\}^T \tag{3}$$

Considering the assumption of linear behavior, the relation between these two terms is defined as:

$$\boldsymbol{\epsilon} = \boldsymbol{b}\boldsymbol{u} \tag{4}$$

The 6×3 matrix $\boldsymbol{b}$ is a differential operator whose expression can be found in [35]. The stress vector is defined by the Hooke's law:

$$\boldsymbol{\sigma} = \boldsymbol{C}\boldsymbol{\epsilon} \tag{5}$$

where $\boldsymbol{C}$ is the 6×6 stiffness matrix of the material.

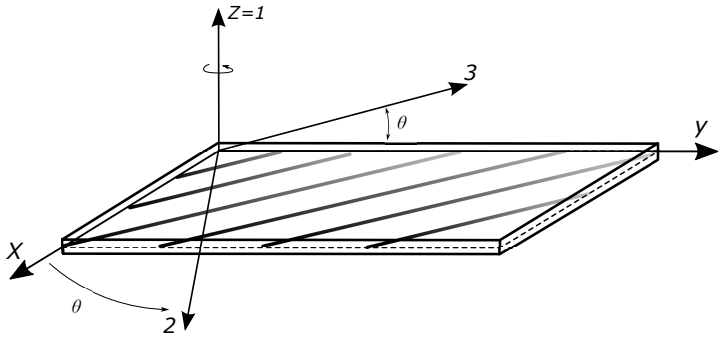

Figure 2: Material reference system

A *anisotropic* material has a different behavior in any direction, and the matrix $\boldsymbol{C}$ is composed of 21 independent coefficients. Instead, if the material is *orthotropic*, the independent terms become nine (considering the symmetry of the components $C_{12} = C_{21}$, $C_{13} = C_{31}$ and $C_{23} = C_{32}$). In this case, the matrix $\boldsymbol{C}$ is defined as:

$$\boldsymbol{C} = \begin{bmatrix} C_{11} & C_{12} & C_{13} & 0 & 0 & 0 \\ C_{21} & C_{22} & C_{23} & 0 & 0 & 0 \\ C_{31} & C_{32} & C_{33} & 0 & 0 & 0 \\ 0 & 0 & 0 & C_{44} & 0 & 0 \\ 0 & 0 & 0 & 0 & C_{55} & 0 \\ 0 & 0 & 0 & 0 & 0 & C_{66} \end{bmatrix} \tag{6}$$

When a composite is considered the fiber may have a general orientation, θ, that is the matrix $\boldsymbol{C}$ should be rotated using a proper rotation matrix, as shown in the book by Reddy [36]:

$$\tilde{\boldsymbol{C}} = \boldsymbol{\Lambda}^T \boldsymbol{C} \boldsymbol{\Lambda} \tag{7}$$

where $\tilde{\boldsymbol{C}}$ is the matrix of the material coefficients in the beam reference system and $\boldsymbol{\Lambda}$ is the rotation matrix.

2.2. Kinematic assumption and FE solution

In the framework of the 1D CUF formulation the displacement field is expressed as the product of two contributions. The first one is the expansion used to describe the behavior over the cross-section. The second contribution is the solution along the beam axis. This product provides a three-dimensional (3D) displacement field expressed in this form:

$$\mathbf{u}(x, y, z) = F_\tau(x, z)\mathbf{u}_\tau(y), \qquad \tau = 1, 2 \dots M, \tag{8}$$

where F_τ is an arbitrary cross-section expansion in function of x and z, while M is the number of the expansion terms. According to the used function F_τ, the kinematics of the model can be profoundly modified. The problem is solved using the FEM method. Introducing the Lagrange function as shape functions N_i, the unknown vector $\mathbf{u}$ is approximated as follows.

$$\mathbf{u}(x, y, z) = F_\tau(x, z)N_i(y)\mathbf{q}_{\tau i} \tag{9}$$

The index i denotes the number of nodes of the beam element and $\mathbf{q}_{\tau i}$ are the nodal unknowns. The expression of the shape functions can be found on [35] .

Using the principle of the virtual work (PVD), the stiffness matrix can be derived. The PVD is expressed as

$$\delta L_{int} = -\delta L_{ine} \tag{10}$$

where δ denotes the virtual variation. The terms of 10 are the variation of the strain energy L_{int} and of the inertial work L_{ine}. Respectively, this two terms can be written as follows:

$$\delta L_{int} = \int_V \delta \boldsymbol{\epsilon}^T \boldsymbol{\sigma} dV \tag{11}$$

$$\delta L_{ine} = \int_V \delta \boldsymbol{u}^T \rho \ddot{\boldsymbol{u}} dV \tag{12}$$

where ρ is the material density, $\ddot{\boldsymbol{u}}$ is the acceleration vector, $\boldsymbol{\sigma}$ is the stress vector and $\delta\boldsymbol{\epsilon}$ is the virtual variation of the strain defined as:

$$\delta\boldsymbol{\epsilon} = \boldsymbol{b}\delta\boldsymbol{u} = \boldsymbol{b}F_s(x,z)N_j(y)\delta\mathbf{q}_{sj} \tag{13}$$

The following form is achieved by substituting in the equation 11 the formulas 5 and 13:

$$\delta L_{int} = \delta\mathbf{q}_{sj}^T \int_V N_j(y)F_s(x,z)\mathbf{b}^T\tilde{C}\mathbf{b}F_\tau(x,z)N_i(y)dV\mathbf{q}_{\tau i} = \delta\mathbf{q}_{sj}^T\mathbf{k}^{ij\tau s}\mathbf{q}_{\tau i} \tag{14}$$

$\mathbf{k}^{ij\tau s}$ is a 3×3 matrix and it is called the *stiffness fundamental nucleus*(FN). This block has the same form, regardless of the kinematic theory introduced in the problem.

$$\begin{aligned} k_{xx}^{\tau sij} =& \tilde{C}_{22}\int_A F_{\tau,x}F_{s,x}dA\int_l N_iN_jdy + \tilde{C}_{66}\int_A F_{\tau,z}F_{s,z}dA\int_l N_iN_jdy \\ &+ \tilde{C}_{44}\int_A F_\tau F_s dA\int_l N_{i,y}N_{j,y}dy; \\ k_{xy}^{\tau sij} =& \tilde{C}_{23}\int_A F_\tau F_{s,x}dA\int_l N_{i,y}N_{j,y}dy + \tilde{C}_{44}\int_A F_{\tau,x}F_s dA\int_l N_iN_{j,y}dy; \end{aligned} \tag{15}$$

Equation 15 reports two terms of the FN where the differential operator is applied, and the material coefficients are extracted from the integral. This last is subdivided in the integral along the axis and the integral over the plane of the cross-section. The other terms are obtained by the permutation of the indexes, and the global stiffness matrix is achieved by varying the indexes i,j,τ and s. From the inertial work, similarly, the *mass fundamental nucleus* can be obtained. More information about the definition of the mass matrix and the procedure to obtain the global stiffness and mass matrix can be found in the book of Carrera *et al.* [35].

Knowing the mass matrix $\mathbf{M}$ and the stiffness matrix $\mathbf{K}$ and according to the notation used in [35], the free undamped problem can be written as:

$$\boldsymbol{M}\ddot{\boldsymbol{A}} + \boldsymbol{K}\boldsymbol{A} = 0 \tag{16}$$

where $\boldsymbol{A}$ is the nodal unknown vector. The natural frequencies ω_i can be computed by solving the eigenvalue problem

$$(-{\omega_i}^2\boldsymbol{M}+\boldsymbol{K})\boldsymbol{A_i}=0 \tag{17}$$

where $\boldsymbol{A_i}$ is the ith eigenvector.

2.3. Taylor expansion based models

The Taylor expansion based models, TE models, use the Taylor expansions as F_τ and F_s to expand the solution from the node of the beam to the cross-section. The TE model allows the accuracy to be improved by increasing the order of the expansion. Considering a TE model of the second order, the displacement field of the term u_x, for example, is expressed as follows:

$$u_x = u_{x_1} + xu_{x_2} + zu_{x_3} + x^2u_{x_4} + xzu_{x_5} + z^2u_{x_6} \tag{18}$$

An overview of the performances of the Taylor models can be found in the work by Carrera *et. al.*[29]

2.4. Lagrange expansion based models

Introducing the Lagrange polynomials, the cross-section response can be described using two-dimensional elements where the unknowns are only the displacement in the nodes. More two-dimensional elements can be used on the cross-section if a proper assembly procedure is adopted. In this way, arbitrary cross-section geometries can be implemented. The interpolation functions are the following where t and s are the coordinates in the natural reference system:

$$\begin{aligned}
F_\tau &= \frac{1}{4}(r^2 + r*r_\tau)(s^2 + ss^\tau) \qquad \tau = 1,3,5,7 \\
F_\tau &= \frac{1}{2}{s^2}_\tau(s^2 + ss_\tau)(1-r^2) + \frac{1}{2}{r^2}_\tau(r^2 - rr_\tau)(1-s^2) \qquad \tau = 2,4,6,8 \\
F_\tau &= (1-r^2)(1-s^2) \qquad \tau = 9
\end{aligned} \tag{19}$$

These functions allow cross-sectional elements with different numbers of nodes (Lagrange Nodes) to be built, each one with three degrees of freedom. In this work, only the nine-node set has been used, and the accuracy of the kinematics has been improved by increasing the number of L9 elements.

LE models allow the laminate to be investigated using a LW approach. This characteristic means that the model considers each layer separately improving the accuracy of the classical methods based on the Equivalent Single Layer (ESL). The cross-sectional discretization defines the layers of the laminate, and for each ply, an arbitrary material and lamination angle can be imposed. In this way, the real description of the laminate can be obtained as shown in Figure 3.

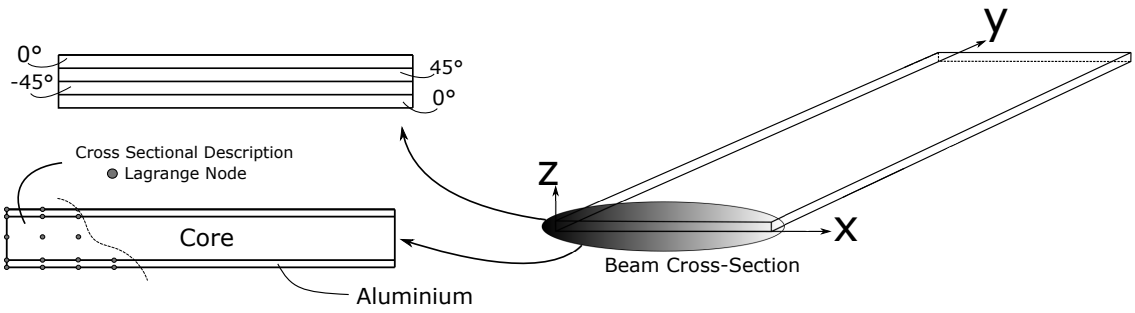

Figure 3: Layer-wise approach description

3. Variable angle tow model

When a variable angle tow structure is considered, the layers of a laminate are no longer characterized by straight fibers rotated by a specific angle but each fiber follows a path that can be arbitrary defined. The fibers of a VAT plate have a continuous variation of the lamination angle, in this way, at each position, the laminate has a different stiffness value. The implementation of a VAT model requires to consider the lamination angle, θ, as a variable in the whole plate domain, that is, the matrix $\tilde{\boldsymbol{C}}$ is no longer constant in each ply but it is function of the coordinates of the point in which is evaluated.

$$\tilde{\boldsymbol{C}} \longrightarrow \tilde{\boldsymbol{C}}(x_G, y_G, z_G) \tag{20}$$

This means that, considering the expression of the FN terms reported in Equation 15, the elastic coefficients, e.g. $\tilde{C}_{22}$, cannot be extracted from the integrals. Besides, the integration along the

beam axis and the integration over the cross-section should be performed simultaneously.

$$
\begin{aligned}
k_{xx}^{\tau sij} &= \int_V \tilde{C}_{22} F_{\tau,x} F_{s,x} N_i N_j dV + \int_V \tilde{C}_{66} F_{\tau,z} F_{s,z} N_i N_j dV \\
&+ \int_V \tilde{C}_{44} F_\tau F_s N_{i,y} N_{j,y} dV; \\
k_{xy}^{\tau sij} &= \int_V \tilde{C}_{23} F_\tau F_{s,x} N_{i,y} N_{j,y} dV + \int_V \tilde{C}_{44} F_{\tau,x} F_s N_i N_{j,y} dV;
\end{aligned}
\tag{21}
$$

The fundamental nucleus reported in Equation 15 can be rewritten in the form reported in Equation 21 where the integrals have been combined in a unique volume integral which includes the material proprieties too. The present implementation refers to the Gauss integration technique to evaluate the integrals. In the case of a classical laminate the first contribution of the first term reported in Equation 15 can be written as:

$$
\begin{aligned}
&\tilde{C}_{22} \int_A F_{\tau,x} F_{s,x} dA \int_l N_i N_j dy = \tilde{C}_{22} \int_{-1}^{1} \int_{-1}^{1} F_{\tau,x} F_{s,x} |J^{2D}| d\eta d\nu \int_{-1}^{1} N_i N_j |J^{1D}| d\xi = \\
&\tilde{C}_{22} \sum_{l=1}^{n_{gp}^l} \sum_{k=1}^{n_{gp}^k} F_{\tau,x}(\eta_l, \nu_k) F_{s,x}(\eta_l, \nu_k) |J^{2D}(\eta_l, \nu_k)| w_l w_k \sum_{m=1}^{n_{gp}^m} N_i(\xi_m) N_j(\xi_m) |J^{1D}(\xi_m)| w_m
\end{aligned}
\tag{22}
$$

where η, ν and ξ are the natural coordinates, $|J^{2D}|$ and $|J^{1D}|$ are the determinants of the Jacobian of the iso-paraemtric transformations over the cross-section and along the beam respectively; w_m, w_l and w_k are the weights related to the Gauss points η_l, ν_k and ξ_m; n_{gp} is the number of the Gauss point used.

In the VAT model the splitting of the integral is not possible,, that is Equation 21 assumes the new form:

$$
\begin{aligned}
&\int_V \tilde{C}_{22} F_{\tau,x} F_{s,x} N_i N_j dV = \int_{-1}^{1} \int_{-1}^{1} \int_{-1}^{1} \tilde{C}_{22} F_{\tau,x} F_{s,x} N_i N_j |J^{2D}||J^{1D}| d\eta d\nu d\xi = \\
&\sum_{l=1}^{n_{gp}^l} \sum_{k=1}^{n_{gp}^k} \sum_{m=1}^{n_{gp}^m} \tilde{C}_{22}(\xi_m, \eta_l, \nu_k) F_{\tau,x}(\eta_l, \nu_k) F_{s,x}(\eta_l, \nu_k) N_i(\xi_m) N_j(\xi_m) |J^{1D}(\xi_m)||J^{2D}(\eta_l, \nu_k)| w_l w_k w_m
\end{aligned}
\tag{23}
$$

where $\tilde{C}_{22}(\xi_m, \eta_l, \nu_k)$ is the material constant evaluated in a specific Gauss point. The evaluation of the new integrals has consequences on the computational cost that should be pointed out. First of all, the order of the function to be integrated is now given by the order of the shape functions and by the order of the law used to describe the fiber path, that is, a proper number of Gauss points should be defined in order to obtain an accurate integral. Moreover, the evaluation of the integral reported in Equation 23 requires $(n_{gp}^l \times n_{gp}^k \times n_{gp}^m)$ loops while the integral in Equation 22 requires

only $(n_{gp}^{l} \times n_{gp}^{k} + n_{gp}^{m})$ loops, that is, an increase of the computational cost of the VAT model with respect to the conventional one has to be expected.

Figure 4 shows the differences between the current VAT model, where the material proprieties are evaluated at each Gauss point, and a Step by Step model usually implemented in the commercial codes and here used in some preliminary assessments. The second approach considers the lamination angle as constant over the whole element. In this case, the Gauss points of the element are characterized by the same material proprieties. Within this assumption, the curvilinear paths of the fibers are approximated by linear segments, that is a higher number of elements is required to describe the fiber paths correctly. This kind of approach is widely used in the commercial softwares, such as in the work of Demasi *et al.*[37] where an expensive solid model is used as the reference solution.

The Step by Step method produces a coarse estimation of the stiffness by imposing the same mean lamination value for the whole element. Otherwise, the present model considers in each Gauss point the real value of the lamination angle guaranteeing a smoother approximation of the stiffness along the investigated component.

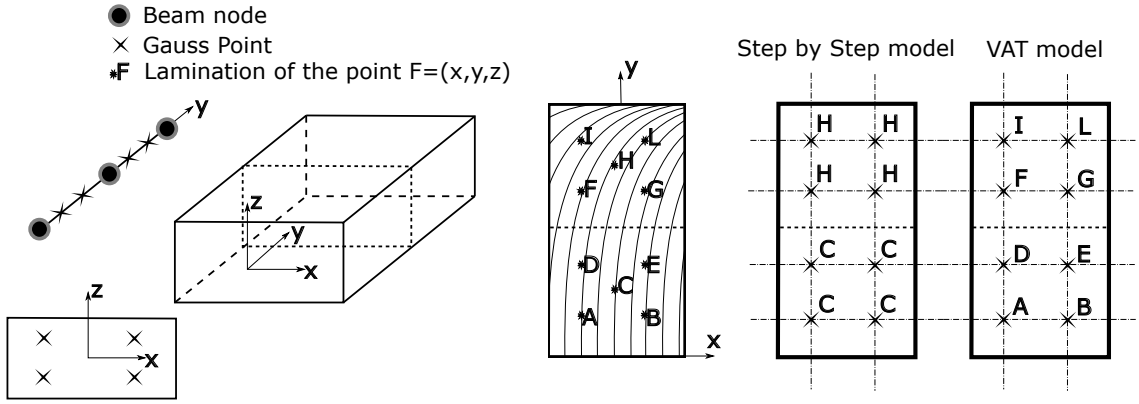

Figure 4: VAT present model vs Step by Step integration scheme

4. Numerical Results

In this section, the present model has been assessed and validated through free vibration analyses. The first part reports an assessment analysis focused on the validation of the current VAT implementation for both the TE and LE models. Convergence analyses have also been performed.

In the second part, the accuracy of the model has been investigated through comparison with literature results, that is a plate has been studied considering different laminations, thickness, and boundary conditions. Finally, a comprehensive comparison between LE and TE based models has been presented.

4.1. Variable angle tow model assessment

The assessments and the convergence analyses of the present model are presented in the current section. A single layer cantilevered plate is considered, see Figure 5. The orthotropic material has the following properties: $E_{LL} = 50\ GPa$, $E_{TT} = E_{ZZ} = 10\ GPa$, $G_{LZ} = G_{TZ} = G_{LT} = 5\ GPa$, $\nu_{LZ} = \nu_{TZ} = \nu_{LT} = 0.25$ and density of 1700 kg/m^3. The lamina has the following dimension:

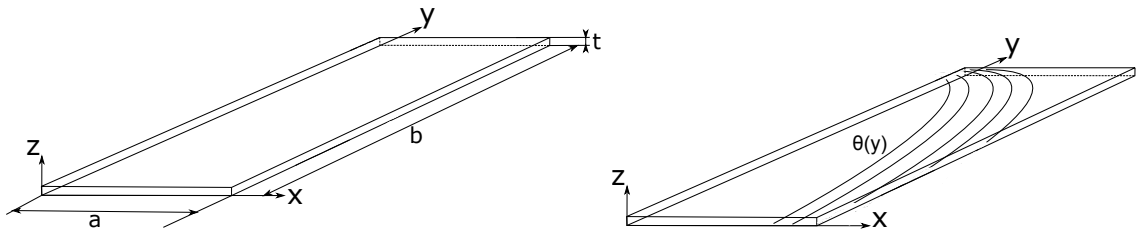

(a) Geometry (b) Lamination

Figure 5: Composite plate considered in the assessment analyses.

$a = 0.2\ m$ and $b = 1\ m$. The thickness t is equal to 0.01 m. The dimensions are shown in Figure 5a. The fibers follow the simple path shown in Figure 5b. At the root the fibers have a lamination angle equal to 0 while that linearly goes to 90 degrees at the free end, as defined in Equation 24.

$$\theta(y) = 0 + \frac{y}{L}90 \tag{24}$$

VAT model VS Step by Step approach

In this section the results obtained with the present model have been compared with those obtained using a step by step approach. The present analysis has been exploited to validate the present approach since a mesh refinement should lead to a convergence between the two models. At the same time, the performances in term of convergence rate of the present VAT model and the classical step by step approach have been investigated. A three dimensional model has been also reported in order to provide a reference solution. The model has been built using a $5 \times 40 \times 3$ mesh

# Beam Element Position	1	2	3	4	5
Angle [°]	9	27	45	63	81

Table 1: Step by step lamination angles for the case of a five beam element mesh.

and hexahedral elements with 27 nodes, H27, have been used. Table 1 reports, as an example, the step by step lamination angles for the case in which a mesh with five beam elements is considered. Different mesh refinements have been considered and the results have been reported in Tab 2. The first 15 natural frequencies have been evaluated using 5, 10, 15, 30 and 60 B3 elements. All the models share the same cross-section kinematic approximation, 4 L9 Lagrange elements. The degrees of freedom of each model have been reported in the second row of Table 2. The four node beam

	Step by Step 4L9 Model					VAT 4L9 Model					3D Model
Model	5B3	10B3	15B3	30B3	60B3	5B3	10B3	15B3	30B3	60B3	600H27
DOF	891	1701	2511	4941	9801	891	1701	2511	4941	9801	18711
Mode 1	6,66	6,59	6,57	6,57	6,57	6,62	6,58	6,57	6,57	6,57	6,56
Mode 2	35,52	34,02	33,76	33,63	33,61	35,57	34,02	33,76	33,63	33,61	33,61
Mode 3	58,47	57,20	56,98	56,89	56,88	58,86	57,28	57,02	56,90	56,88	56,70
Mode 4	105,60	94,76	92,96	92,09	91,98	105,78	94,71	92,95	92,09	91,98	91,94
Mode 5	124,44	124,51	124,58	124,62	124,63	124,83	124,68	124,66	124,65	124,64	124,62
Mode 6	166,50	159,16	157,69	156,89	156,77	166,50	159,29	157,73	156,89	156,77	156,40
Mode 7	242,98	192,93	186,79	183,92	183,53	243,97	192,53	186,64	183,91	183,53	183,34
Mode 8	303,05	280,05	274,90	271,76	271,26	304,29	280,73	275,16	271,78	271,26	270,74
Mode 9	387,20	330,66	315,47	308,87	307,99	389,52	329,80	315,10	308,84	308,00	307,52
Mode 10	483,90	418,11	407,68	401,39	400,38	490,27	419,20	408,15	401,45	400,38	399,53
Mode 11	529,56	508,69	473,37	458,05	456,00	529,75	507,72	472,84	458,00	456,01	455,43
Mode 12	750,98	527,14	526,94	526,88	526,87	741,82	527,20	526,98	526,89	526,87	526,77
Mode 13	854,97	581,86	560,90	549,61	547,81	852,73	583,35	561,57	549,69	547,82	546,52
Mode 14	871,40	729,77	663,18	632,51	628,34	871,64	729,42	662,58	632,45	628,35	627,84
Mode 15	1131,43	784,90	739,07	718,04	714,88	1136,81	786,90	739,99	718,17	714,89	713,13

Table 2: First 15 natural frequencies of the cantilevered plate calculated using a Step by Step description and a VAT model. B3 elements have been used.

elements (B4) have been also considered, In this case, the following meshes have been used: 10, 20

and 60 B4 elements. Table 3 shows the results obtained with these models.

	Step by Step 4L9 Model			VAT 4L9 Model		
Model	10B4	20B4	60B4	10B4	20B4	60B4
DOF	2511	4941	14661	2511	4941	14661
Mode 1	6,56	6,56	6,57	6,57	6,57	6,57
Mode 2	33,63	33,61	33,61	33,62	33,61	33,61
Mode 3	56,85	56,87	56,88	56,90	56,88	56,88
Mode 4	91,97	91,96	91,96	92,01	91,97	91,96
Mode 5	124,45	124,59	124,63	124,65	124,64	124,64
Mode 6	157,04	156,82	156,75	156,83	156,77	156,75
Mode 7	183,54	183,48	183,48	183,68	183,51	183,49
Mode 8	271,80	271,30	271,20	271,59	271,25	271,20
Mode 9	308,23	307,91	307,89	308,53	307,97	307,90
Mode 10	401,46	400,42	400,25	401,25	400,36	400,25
Mode 11	457,18	455,85	455,76	457,69	455,94	455,78
Mode 12	526,77	526,84	526,86	526,92	526,88	526,86
Mode 13	549,77	547,86	547,58	549,68	547,81	547,58
Mode 14	631,94	628,11	627,87	632,71	628,24	627,89
Mode 15	718,44	714,91	714,49	718,44	714,88	714,49

Table 3: First 15 natural frequencies of the cantilevered plate calculated using a Step by Step description and a VAT model. B4 elements have been used.

Figures 6*a-f* reproduce the convergence of the models considered for the first six modes. The figures report on the x-axis the degrees of freedom that depend on the number of beam elements used. On the y-axis is reported the frequency value. The results underline the convergence behavior of the two approaches and confirm the capability of the VAT model to converge faster than the classical approach. The curves show how, at equal degrees of freedom, the VAT models introduce a lower error compared to a Step by Step model. In this case, considering the simple fiber pattern, the advantages of the present model are small compared to the Step by Step approach, but it is clear as, even with few element, the VAT model is able to produce results more accurate. The xy-bending mode, mode 5, has a different convergence because of the stepped model underestimates the stiffness at the root of the lamina, that is, for a coarse mesh a lower frequency value is predicted.

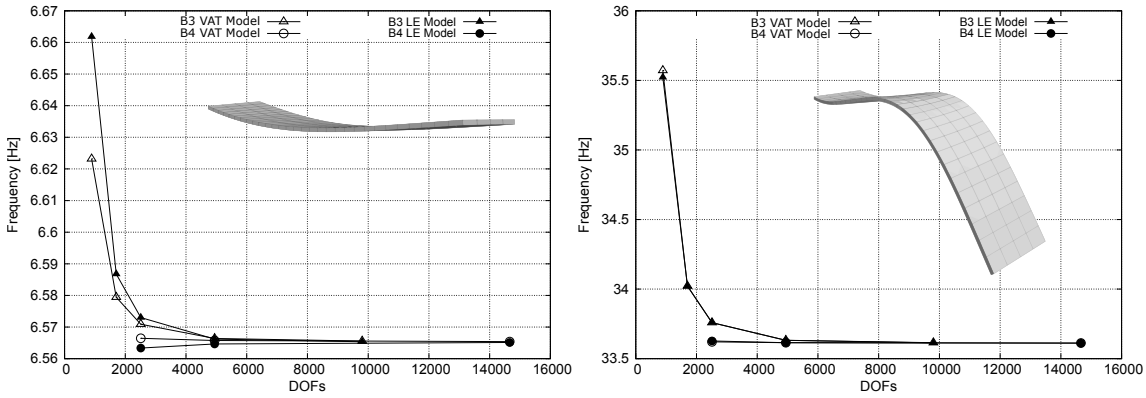

(a) Mode 1

(b) Mode 2

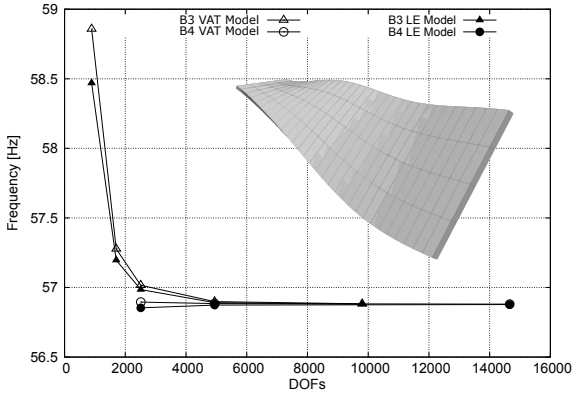

(c) Mode 3

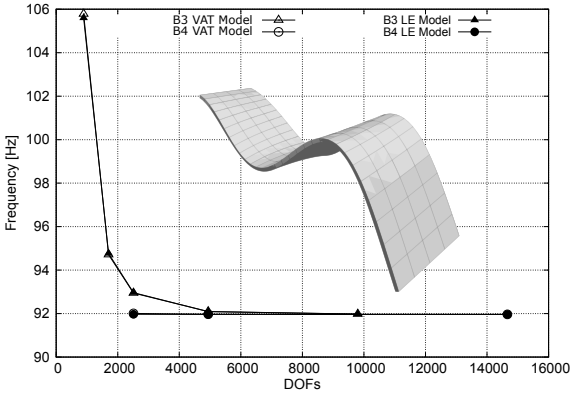

(d) Mode 4

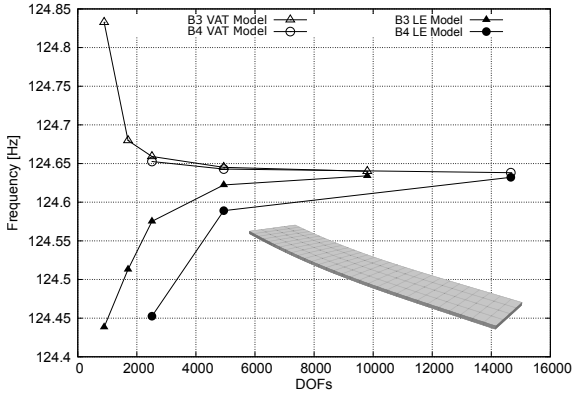

(e) Mode 5

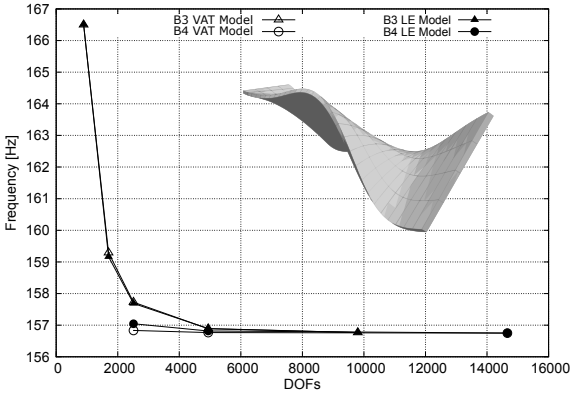

(f) Mode 6

Figure 6: Convergence analysis of the first six natural frequencies

Comparison between LE and TE models

In this section the effect of the cross-section kinematic approximation is investigated. LE and TE models have been compared considering different cross-sectional meshes, in the case of LE models, and different expansion orders, when TE models have been considered. Table 4 shows the values obtained using the two expansions at different refinement levels. The results refer to a model with ten B3 elements along the axis.

Columns 2 to 6 report the results obtained from a refinement of the cross-sectional mesh for the LE models, that is a higher number of Lagrange elements is considered. As shown by the results, the refinement leads to weak improvements, also at high frequencies.

A different behaviors can be appreciated when the model uses TE expansions, see column 7 to 12. The classical theories (Eulero Bernoulli as EULE and Timoshenko as TBT) present the well-known limitations due to their fundamental assumptions. The bending modes have been correctly predicted but the torsional modes as well as the effects due to the bending/torsional coupling effects have not been detected as shown in figure 7. The first order TE model does not introduce sensible improvements. The second order model appear to be more accurate, the errors on the frequency values have a sensible decrease, and the torsional effects are detected. The fourth order model is able to provide an excellent accuracy comparable with the 4L9 model but with the half of DOFs.

In conclusion it is clear that accurate results for VAT beam structure can be obtained only using an higher order model. Both TE and LE models have provided accurate results in the case of a structure with only one layer. The following section will consider more realistic cases and more complex lamination schemes.

4.2. Analysis of a multilayered VAT panel

In this section outcomes of [22] are used to compare the present VAT model with literature results. The reference uses a p-version finite element based on the TSDT. The studied case concerns the plate shown in Figure 8 characterized by the following dimensions: $a = b = 1\ m$. Two thicknesses are considered: $0.01\ m$ and $0.1\ m$ respectively for thin and thick plates. The plate is a three-layer laminate, and the lamination of each layer will be expressed as $< T_0, T_1 >$, where T_0 and T_1 are the two parameters used to identify the lamination angle as expressed in Equation 25. The plate is described using a LE model which allows a LW approach to be employed. 10 B3 elements are used over the $y - axis$, and 30 9-node Lagrange Elements are used to describe the

	VAT 10B3 LE Model					VAT 10B3 TE Model					
Model	2L9	4L9	6L9	8L9	10L9	EULE	TBT	Order 1	Order 2	Order 3	Order 4
DOF	945	1701	2457	3213	3969	189	189	189	378	630	945
Mode 1	6,58	6,58	6,58	6,58	6,58	7,22	7,22	7,22	6,65	6,58	6,58
Mode 2	34,06	34,02	34,01	34,01	34,01	35,04	34,94	34,93	34,34	34,05	34,01
Mode 3	57,53	57,28	57,12	57,02	56,96	96,80	96,13	96,09	59,43	57,71	57,42
Mode 4	94,88	94,71	94,66	94,63	94,62	142,97	137,52	136,14	96,16	94,90	94,63
Mode 5	124,78	124,68	124,67	124,67	124,67	193,27	190,82	190,72	125,57	124,74	124,69
Mode 6	159,87	159,29	158,92	158,68	158,53	330,13	323,43	323,23	166,78	160,31	159,58
Mode 7	193,03	192,53	192,35	192,25	192,19	515,78	500,44	429,04	197,35	193,39	192,37
Mode 8	281,88	280,73	280,05	279,64	279,38	657,71	548,72	500,06	300,63	283,25	281,29
Mode 9	330,85	329,80	329,41	329,21	329,09	760,23	729,66	541,73	342,96	332,06	329,49
Mode 10	421,19	419,20	418,08	417,45	417,06	936,30	873,43	729,03	460,29	425,04	420,28
Mode 11	509,37	507,72	507,13	506,84	506,67	1073,13	1018,46	737,83	523,89	511,36	507,11
Mode 12	528,28	527,20	527,06	527,03	527,02	1465,57	1252,97	1017,38	535,10	527,74	527,35
Mode 13	586,62	583,35	581,72	580,87	580,36	1685,49	1418,38	1220,23	651,74	594,83	584,98
Mode 14	732,06	729,42	728,32	727,79	727,48	1690,62	1565,04	1286,86	752,29	735,63	729,22
Mode 15	794,79	786,90	783,95	782,67	782,02	2477,18	2075,31	1417,79	872,17	808,34	788,90

Table 4: First 15 natural frequencies of the VAT plate evaluated using various TE an LE models.

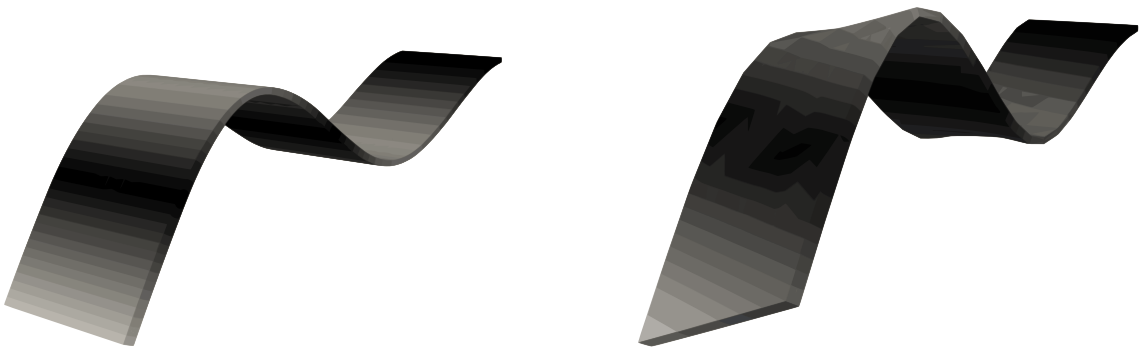

(a) Euelero-Bernulli theory: 96,80 Hz

(b) VAT LE Model: 94,71 Hz

Figure 7: Comparison between Eulero-Bernulli theory and 4L9 model.

cross-section of the plate (10 L9 elements for each layer). Two laminations have been considered.

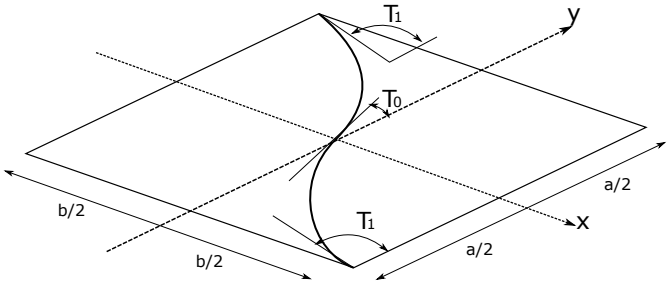

Figure 8: Plate geometry and lamination parameters

The first one, called lamination a, is represented by the following T_0 and T_1 set: $< 0°, 45° >, < -45°, -60° >, < 0°, 45° >$. The second one, lamination b, is always a symmetric lamination and is defined as follows: $< 90°, 45° >, < 60°, 30° >, < 90°, 45° >$.

$$\theta(y) = 2(T_1 - T_0)\frac{|y|}{a} + T_0 \tag{25}$$

Figure 9 presents an example of the previous laminations in order to understand the patterns of the fibers in each layer. It should be noticed that lamination b can introduce some issues in the manufacturing process because of the presence of overlapped fibers at $y = 0$, but this problem is not the topic of this paper. The plate has been analyzed considering two different boundary conditions. At first, the four edges have been supposed clamped while, in a second time, the square plate has been supposed entirely free. A refined three-dimensional solution obtained using a 3D FEM model with $20 \times 20 \times 3$ H27 elements has been included as reference. The 3D model uses a step by step approach and has $\sim$ 95000 DOFs. Table 5 shows the first nine frequency values for the clamped plate. The values confirm the capability of the present model to deal with complex laminate where a VAT lamination characterizes several layers. The results for the thick plate show a higher accuracy while the thin plate presents errors of about some percentage points which can be decreased through a refinement of the cross-sectional mesh. Table 6 shows the results considering the second boundary condition, the free plate. The achieved values agree with those from the reference.

When the thinner panels are considered, the present model shows some discrepancy with respect to the literature results as well as the 3D model, this is due to the high flexibility of the structure that requires a refined cross-sectional kinematic to be well captured. Because of this, a refinement of the cross-sectional discretization leads to a better solution.

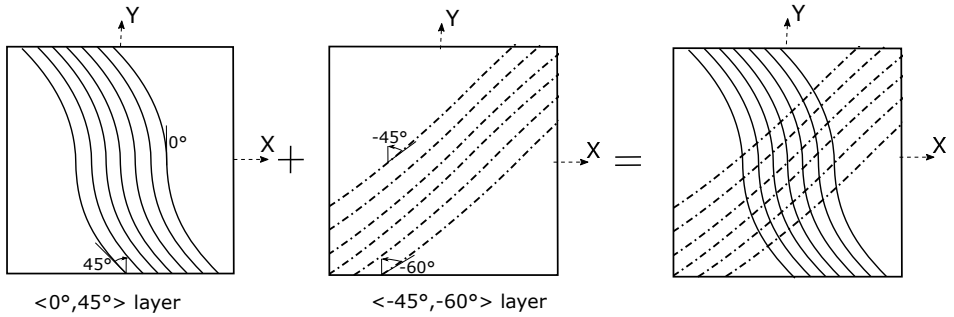

(a) Lamination a

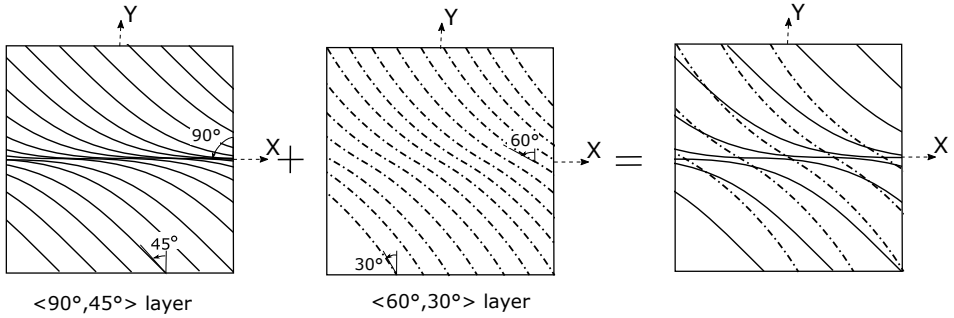

(b) Lamination b

Figure 9: Example of the lamination layups.

h/a		Mode 1	Mode 2	Mode 3	Mode 4	Mode 5	Mode 6	Mode 7	Mode 8	Mode 9
					$[<0,45>,<-45,-60>,<0,45>]$					
0,01	Ref. [22]	92,26	130,82	195,19	237,86	274,99	282,67	340,09	389,10	431,02
	LE Model	94,44	135,36	206,40	247,05	287,67	307,89	361,64	433,83	476,36
	Refined LE Model	92,90	132,28	198,97	240,46	278,75	291,12	346,60	404,07	444,97
	3D Model	92.65	131.50	196.86	239.23	276.76	286.34	342.84	395.43	436.74
0,1	Ref. [22]	614,11	909,55	1233,02	1338,63	1485,64	1798,60	1932,28	1965,59	2152,26
	LE Model	609,79	903,63	1216,00	1328,41	1469,33	1774,84	1930,15	1931,36	2113,88
	3D Model	607.24	897.04	1208.40	1314.14	1458.18	1753.52	1916.57	1904.91	2096.64
					$[<90,45>,<60,30>,<90,45>]$					
0.01	Ref. [22]	113,18	145,25	212,66	269,06	292,47	316,49	362,78	392,79	465,04
	LE Model	114,32	148,92	223,15	279,60	303,80	332,45	381,32	425,44	507,54
	3D Model	113.02	145.21	212.99	269.67	292.70	315.84	358.88	393.29	465.73
0.1	Ref. [22]	682,20	917,49	1304,68	1313,59	1466,64	1714,97	1920,80	1991,02	2001,10
	LE Model	672,68	909,02	1270,07	1301,02	1441,95	1690,38	1904,58	1943,18	1943,44
	3D Model	670.27	904.11	1264.63	1291.94	1433.44	1678.67	1883.04	1931.44	1947.36

Table 5: Natural frequencies [Hz] for the clamped plates.

h/a		Mode 1	Mode 2	Mode 3	Mode 4	Mode 5	Mode 6	Mode 7	Mode 8	Mode 9
					$[<0,45>,<-45,-60>,<0,45>]$					
0,01	Ref. [22]	22,44	27,1	54,87	76,05	94,35	114,01	114,47	138,89	160,49
	LE Model	22,53	27,32	55,03	77,71	94,8	114,76	115,66	140,64	166,68
	3D Model	22.26	27.04	54.39	75.73	93.65	113.60	112.99	137.56	159.39
0,1	Ref. [22]	201,89	258,71	467	664,96	764,44	867,89	903,61	1021,75	1129,86
	LE Model	200,85	257,1	465,16	661,13	759,03	863,08	894,21	1015,21	1122,93
	3D Model	200.28	256.20	462.22	657.30	754.14	858.41	887.09	1009.03	1122.09
					$[<90,45>,<60,30>,<90,45>]$					
0,01	Ref. [22]	19,61	24,1	44,19	62,03	64,41	91,98	99,1	110,45	133,78
	LE Model	19,61	24,25	44,31	62,99	64,81	93,29	101,01	111,26	135,06
	3D Model	19.54	24.09	44.12	62.11	64.35	91.76	99.11	110.19	133.05
0,1	Ref, [22]	182,64	230,91	392,83	560,4	561,81	765,73	837,24	881,66	1010,19
	LE Model	182,02	230,43	392,43	561,63	559,04	764,02	837,75	879,58	987,54
	3D Model	181.46	230.06	391.74	560.02	557.96	760.90	834.15	877.64	986.12

Table 6: Natural frequencies [Hz] for free plates.

When the thicker panels are considered the advantages of a Layer-wise description are more evident, in fact, the results obtained by means of the present model are in agreement with those of the 3D solution while the results reported by Akhavan and Ribeiro [22] have a larger error.

The results show a higher stiffness of the lamination a in the clamped case while, when no boundary conditions are applied, the lamination b is more rigid. This phenomenon is due to the path of the fiber with respect to the modal shapes which are influenced by the boundary conditions. The first modal configuration is considered to explain it. In the clamped case, the lamination b has the fibers perpendicular to the border at $y = 0$, and this feature increases the bending stiffness while the lamination a has only angled fibers at the edges. This distribution of the fibers brings the lamination b to have higher frequencies. In the free condition, the angled fibers (particularly $+-45°$ fibers) govern the modal shape. Lamination a is very close to a $(+45°, -45°, +45°)$ lamination and provides a greater stiffness with respect to the lamination b. Figure 10 shows the first five modal shapes of the clamped panel for both the laminations.

Figure 11 presents the modal shapes in the case of the free boundary condition. The correct description of the VAT lamination can be noted in the first modal shape. In fact, in the lamination a there is a quasi-symmetric modal shape because of a quasi-$+45°/-45°$ lamination. Instead, the lamination b has two corners that moves more than the others because along with a diagonal the most of the fibers are perpendicular, so in this direction, the plate is less rigid. This can be better explained using the figure 12 which shows that the top-right and bottom-left corner have no longitudinal fibers over the conjunction line, and, in fact, they have a more significant displacement.

4.3. Layer-Wise VS Equivalent Single Layer approach

The present section aims to compare the LE and TE models in the case of a complex lamination such as the one considered in the previous section. LE models are able to provide a Layer-wise description since each layer has a proper description while the TE models introduce a global expansion that leads to an Equivalen Single Layer approach. Table 7 presents the frequencies achieved by the analysis of the previous free plate with the thickness equal to 0.01 m.

The frequency values show that the first order TE model presents difficulties in the correct detection of the vibrational behavior of the plate. Higher order models provide more accurate results, especially when lamination b is considered.

A more exhaustive analysis can be done comparing the modal shapes evaluated using different

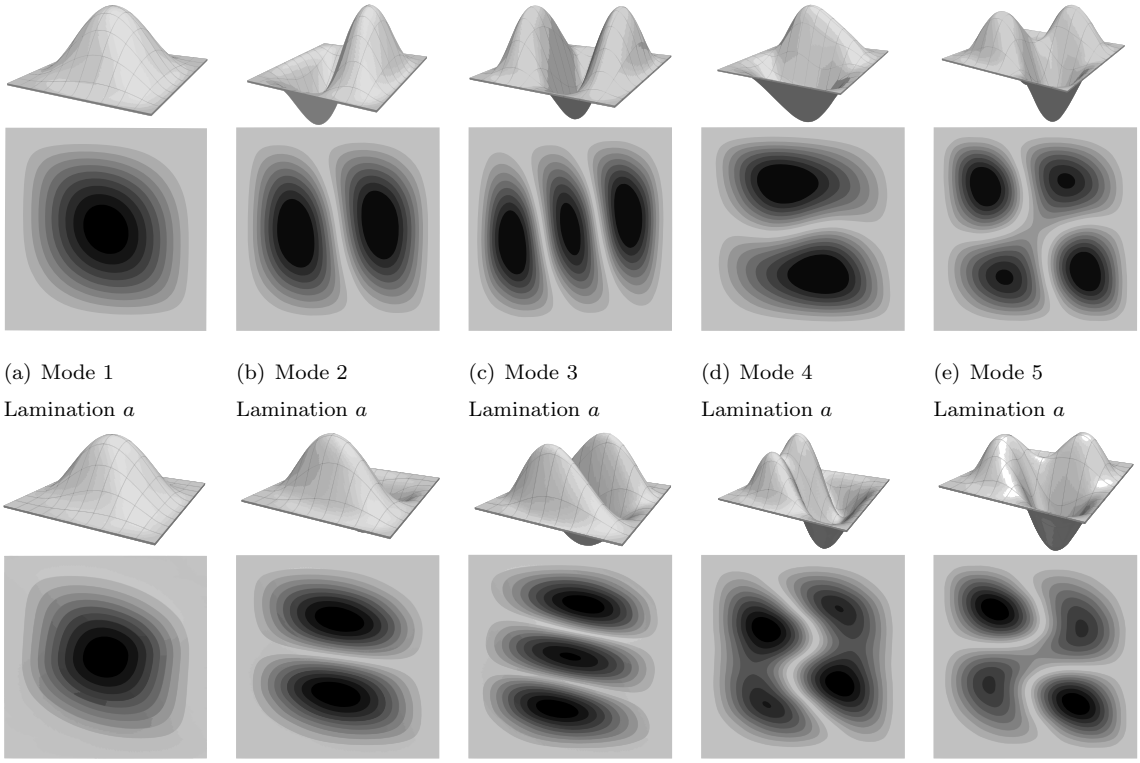

(a) Mode 1
Lamination a

(b) Mode 2
Lamination a

(c) Mode 3
Lamination a

(d) Mode 4
Lamination a

(e) Mode 5
Lamination a

(f) Mode 1
Lamination b

(g) Mode 2
Lamination b

(h) Mode 3
Lamination b

(i) Mode 4
Lamination b

(j) Mode 5
Lamination b

Figure 10: First 5 modal shapes of the clamped plate.

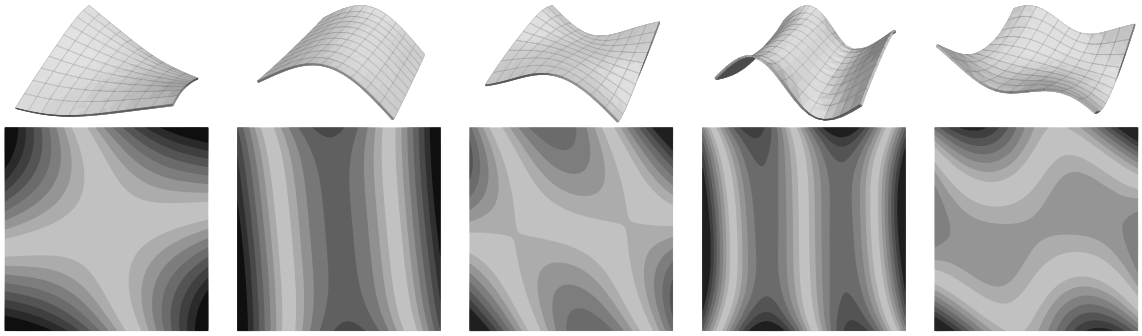

(a) Mode 1 Lamination a (b) Mode 2 Lamination a (c) Mode 3 Lamination a (d) Mode 4 Lamination a (e) Mode 5 Lamination a

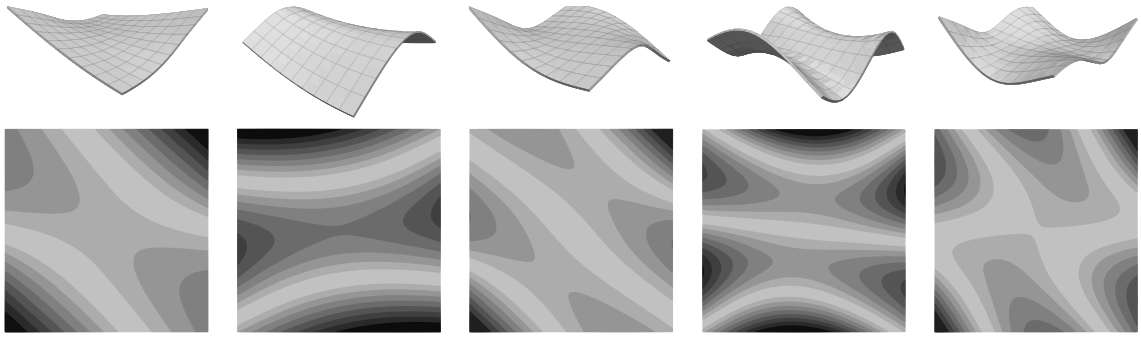

(f) Mode 1 Lamination b (g) Mode 2 Lamination b (h) Mode 3 Lamination b (i) Mode 4 Lamination b (j) Mode 5 Lamination b

Figure 11: First 5 modal shapes of the free thin plate.

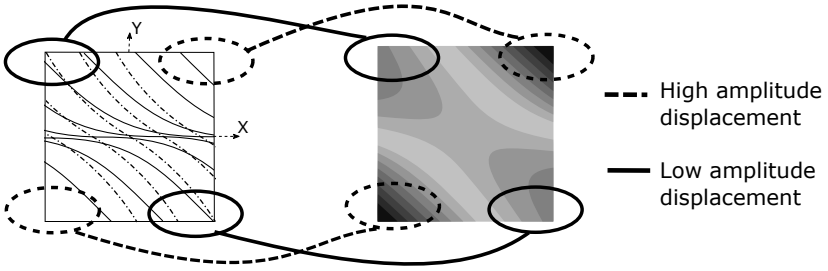

Figure 12: Effects of the fiber placements on the 1^{st} free modal shape.

models. The Modal Assurance Criterion [38] has been used to compare the modal shapes. When the MAC has a value equal to 1 there is a perfect modal matching while a value equal to 0 means complete mismatching, intermediate values represent a partial correspondence between the modal shapes. These values can be reported on the colored matrix shown in the Figures 13 and 14 where a black square represents two identical modal forms. Figures 13 and 14 report the results for lamination a and lamination b respectively. Two models have a perfect correlation if these graphs are characterized by a black diagonal.

Figure 13 shows that when lamination a is considered even a fourth order model is not able to detect correctly the modal shapes, in fact it can be noticed a modal switch between the fourth and the fifth mode. Moreover, modes six, seven and eight show some contamination since some values out of the diagonal are nor perfectly zero. Figure 14 shows that ESL models perform better when lamination b is considered. A third order model is able to detect the first five modal shape while a fourth order model detects accurately the first eight modal shapes.

It can be concluded that, when complex laminations are considered, the use of refined models is mandatory. A LW approach leads to accurate results but it also requires a higher computational cost. Despite the ESL models are not as accurate as the LW ones, they can lead to a strong reduction in the computational cost.

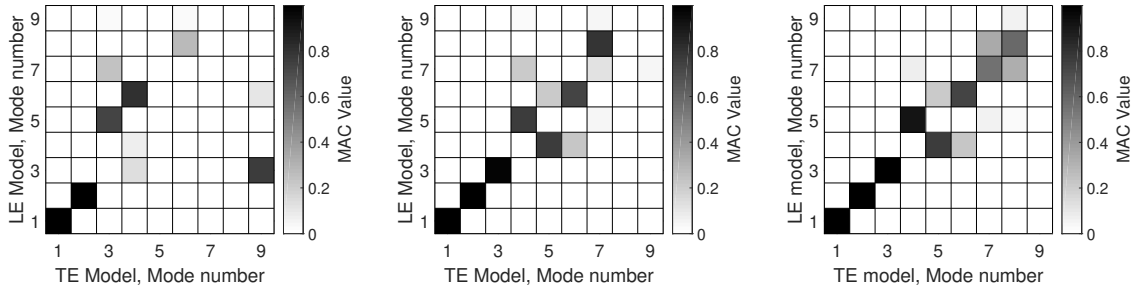

(a) 2^{nd} order TE Model (b) 3^{rd} order TE Model (c) 4^{th} order TE Model

Figure 13: Modal shapes comparison between the LE model and different orders of the TE model for the lamination a

Model	Mode 1	Mode 2	Mode 3	Mode 4	Mode 5	Mode 6	Mode 7	Mode 8	Mode 9
$[<0,45>,<-45,-60>,<0,45>]$									
LE Model	22,53	27,32	55,03	77,71	94,8	114,76	115,66	140,64	166,68
TE Model 1^{st} order	92,17	205,38	376,48	620,37	723,38	785,14	781,33	934,10	1326,02
TE Model 2^{nd} order	23,50	31,87	104	111,65	266,91	267,54	497,23	500,81	779,24
TE Model 3^{rd} order	23,18	31,86	62,12	101,63	103,67	129,95	146,55	267,56	302,78
TE Model 4^{th} order	22,77	27,49	59,08	98,34	101,06	129,63	139,42	152,68	210,75
$[<90,45>,<60,30>,<90,45>]$									
LE Model	19,61	24,25	44,31	62,99	64,81	93,29	101,01	111,26	135,06
TE Model 1^{st} order	22,68	64,69	131,36	225,23	350,20	511,06	710,84	781,29	1097,91
TE Model 2^{nd} order	20,33	24,61	57,28	92,49	94,17	110,18	186,16	196,98	303,67
TE Model 3^{rd} order	20,07	24,48	46,51	64,35	78,04	106,76	110,70	161,71	172,32
TE Model 4^{th} order	19,75	24,31	45,11	63,74	66,88	97,79	101,33	121,16	172,32

Table 7: Comparison between LE model (Layer-wise approach) with TE models (Equivalent Single Layer)

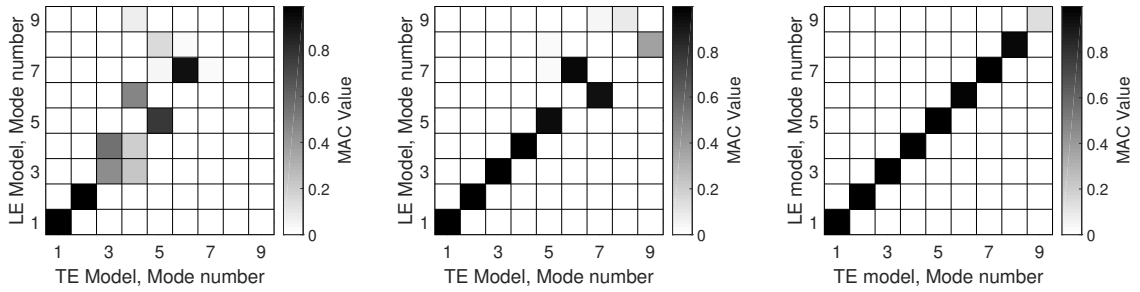

(a) 2^{nd} order TE Model (b) 3^{rd} order TE Model (c) 4^{th} order TE Model

Figure 14: Modal shapes comparison between the LE model and different orders of the TE model for the lamination *b*

5. Conclusions

In this work, a refined beam model based on the Carrera Unified Formulation has been extended to the free vibration analysis of plates made of VAT composites. A new approach in evaluation of the stiffness matrix has been introduced in order to include a variable lamination angle within the same layer. Single- and Multi-layer plates have been considered using both layer-wise and equivalent single layer approaches. An extensive validation of the models has been performed considering the effects of the finite element discretization as well as the cross-sectional kinematic approximation. The present VAT model has been compared with a Step by Step model and the convergence of both the approaches has been investigated. The model has been then compared with other approaches presented in literature. Multi-layer plates with complex fiber patterns have been investigated considering different boundary conditions and geometrical configurations. The results lead to the following remarks:

- the present VAT model is able to detect the effects due to curvilinear fibers as proven by the comparison with the results obtained from a step by step approach and open literature;
- the introduction of curvilinear fibers in a lamina can introduce complex coupling effects that cannot be detected by the classical theories, that is refined models are required;
- the use of VAT composite materials allows the stiffness to be arbitrarily distributed over a panel, that is, an accurate design can lead to desired frequencies and modal shapes;
- the use of ESL models, justified by their lower computational cost, can be considered only when thin panels are considered. Despite their higher computational cost, the LW models provide accurate results even when thick panels are considered;
- for a given TE model a different lamination layup may lead to a different accuracy level that is Layer-wise models are strongly recommended when VAT structures have to be investigated.

The advantages of the use of variable angle tow composite materials may lead to more performing design solutions as long as appropriate numerical tools are used in the design process. The present work shows that refined one-dimensional models are an accurate and reliable approach to the design of such structures.

References

[1] A. Leissa, A. Martin, Vibration and buckling of rectangular composite plates with variable fiber spacing, Composite Structure 14 (4) (1990) 339–357. doi:https://doi.org/10.1016/0263-8223(90)90014-6.

[2] M. DiNardo, P. Lagace, Buckling and postbuckling of laminated composites with ply drop-offs, AIAA Journal 27 (10) (1989) 1392–1398. doi:https://doi.org/10.2514/3.10276.

[3] H. Dirk, C. Ward, K. Potter, The engineering aspects of automated prepreg layup: History, present and future, Composites: Part B 43 (3) (2012) 997–1009. doi:10.1016/j.compositesb.2011.12.003.

[4] R. Hyer, M.W. Charette, The use of curvilinear fiber format in composite structure design, 30th Conference on structures, structural dynamics and materials.

[5] R. Hyer, M.W. Charette, Use of curvilinear fiber format in composite structure design, AIAA Journal 29 (6) (1991) 1011–1015. doi:10.2514/3.10697.

[6] M. Hyer, H. Lee, The use of curvilinear fiber format to improve buckling resistance of composite plates with central circular holes, Composite Structures 18 (3) (1991) 239–261. doi:10.1016/0263-8223(91)90035-W.

[7] C. Waldhart, Analysis of tow-placed, variable-stiffness laminates., Master of Science dissertation Virginia Tech.

[8] T. Langley, Finite element modeling of tow-placed variable-stiffness composite laminates., Master of Science dissertation Virginia Tech.

[9] B. Tatting, Analysis and design of variable stiffness composite cylinders., Master of Science dissertation Virginia Tech.

[10] B. Tatting, Z. Grdal, Design and manufacture of elastically tailored tow placed plates.., NASA/CR-2002-211919.

[11] C. Lopes, P. Camanho, Z. Grdal, B. Tatting, Progressive failure analysis of tow-placed variable-stiffness composite panels, International Journal of Solids and Structures 44 (25-26) (2007) 8493–8516. doi:10.1016/j.ijsolstr.2007.06.029.

[12] O. Stodieck, J. Cooper, P. Weaver, P. Kealy, Improved aeroelastic tailoring using tow-steered composites, Composite Structures 106 (2013) 703–715. doi:10.1016/j.compstruct.2013.07.023.

[13] C. Xiaodong, W. Zhangming, N. Guojun, P. Weaver, Buckling analysis of variable angle tow composite plates with a through-the-width or an embedded rectangular delamination., International Journal of Solids and Structures 138 (2018) 166–180. doi:10.1016/j.ijsolstr.2018.01.010.

[14] W. Zhangming, G. Raju, P. Weaver, Postbuckling analysis of variable angle tow composite plates, International Journal of Solids and Structures 50 (10) (2013) 1770–1780. doi:10.1016/j.ijsolstr.2013.02.001.

[15] Z. Wu, P. Weaver, G. Raju, B. Kim, Buckling analysis and optimisation of variable angle tow composite plates, Thin-Walled Structures 60 (2012) 163–172. doi:10.1016/j.tws.2012.07.008.

[16] W. Zhangming, G. Raju, P. Weaver, Optimization of postbuckling behaviour of variable thickness composite panels with variable angle tows: Towards Buckle-Free design concept, International Journal of Solids and Structures 132-133 (2018) 66–79. doi:10.1016/j.ijsolstr.2017.08.037.

[17] C. Xiaodong, W. Zhangming, N. Guojun, P. Weaver, Buckling analysis of variable angle tow composite plates with a through-the-width or an embedded rectangular delamination., International Journal of Solids and Structures 138 (2018) 166–180. doi:10.1016/j.ijsolstr.2018.01.010.

[18] P. Ribeiro, H. Akhavan, Non-linear vibrations of variable stiffness composite laminated plates, Composite Structures 94 (8) (2012) 2424–2432. doi:10.1016/j.compstruct.2014.07.007.

[19] P. Ribeiro, Non-linear free periodic vibrations of variable stiffness composite laminated plates, Nonlinear Dynamics 70 (2) (2012) 1535–15482. doi:10.1007/s11071-012-0554-4.

[20] M. Montemurro, A. Catapano, On the effective integration of manufacturability constraints within the multi-scale methodology for designing variable angle-tow laminates, Composite Structures 161 (2017) 145–159. doi:10.1016/j.compstruct.2016.11.018.

[21] X. Zhou, P. D. Gosling, Towards an understanding of variations in the buckling of tailored variable angle tow composite plates, Composite Structures 203 (2018) 797–809. doi:10.1016/j.compstruct.2018.07.061.

[22] H. Akhavan, P. Ribeiro., Natural modes of vibration of variable stiffness composite laminates with curvilinear fibers, Composite Structures (93) (2011) 3040–3047.

[23] S. Yazdani, P. Ribeiro., A layerwise p-version finite element formulation for free vibration analysis of thick composite laminates with curvilinear fibres, Composite Structures 120 (1) (2015) 531–542. doi:10.1016/j.compstruct.2014.10.030.

[24] S. Yazdani, P. Ribeiro., Geometrically non-linear static analysis of unsymmetric composite plates with curvilinear fibres: p-version layerwise approach, Composite Structures 118 (2015) 74–85. doi:10.1016/j.compstruct.2014.07.007.

[25] D. Robbin, J. Reddy, Refined Beam Elements With Only Displacement Variables and Plate/Shell Capabilities., International Journal for Numerical Methods in Engineering 36 (4) (1993) 655–677.

[26] R. Shimpi, A. Ainapure, A beam finite element based on layerwise trigonometric shear deformation theory., Composite Structures 53 (2) (2001) 153–162.

[27] E. Carrera, Developments, ideas, and evaluations based upon Reissner's Mixed Variational Theorem in the modeling of multilayered plates and shells., Appl. Mech. Rev 54 (4) (2001) 301–329. doi:10.1115/1.1385512.

[28] E. Carrera, Theories and finite elements for multilayered plates and shells: a unified compact formulation with numerical assessment and benchmarking., Archives Comput Methods 10 (3) (2003) 215–296.

[29] E. Carrera, G. Giunta, P. Nali, M. Petrolo, Refined Beam Elements With Arbitrary Cross-Section Geometries, Comput. Struct. 88 (5–6) (2010) 283–293.

[30] M. Petrolo, E. Zappino, E. Carrera, Refined free vibration analysis of onedimensional structures with compact and bridge-like cross-sections., ThinWalled Struct 56 (2012) 49–61. doi:10.1016/j.tws.2012.03.011.

[31] A. Pagani, M. Boscolo, J. Banerjee, E. Carrera, Exact dynamic stiffness elements based on one-dimensional higher-order theories for free vibration analysis of solid and thin-walled structures., Journal of Sound and Vibration 332 (23) (2013) 6104–6127. doi:10.1016/j.jsv.2013.06.023.

[32] E. Carrera, M. Petrolo, Refined Beam Elements With Only Displacement Variables and Plate/Shell Capabilities., Meccanica 47 (3) (2012) 537–556.

[33] M. Filippi, A. Pagani, M. Petrolo, G. Colonna, E. Carrera, Static and free vibration analysis of laminated beams by refined theory based on Chebyshev polynomials., Composite Structures 177 (2017) 54–79. doi:doi.org/10.1016/j.compstruct.2017.06.033.

[34] A. Pagani, M. De Miguel, A.G.and Petrolo, E. Carrera, Analysis of laminated beams via unified formulation and Legendre polynomial expansions., Composite Structures 156 (2016) 78–92. doi:10.1016/j.compstruct.2016.01.095.

[35] E. Carrera, M. Cinefra, M. Petrolo, E. Zappino, Finite Element Analysis of Structures Through Unified Formulation, John Wiley & Sons, 2014.

[36] J. Reddy, Mechanics of laminated composite plates and shells. Theory and Analysis, 2nd Edition, CRC Press, 2004.

[37] L. Demasi, G. Biagini, F. Vannucci, E. Santarpia, R. Cavallaro, Equivalent Single Layer, Zig-Zag, and Layer Wise theories for variable angle tow composites based on the Generalized Unified Formulation., Composite Structures 138 (2018) 166–18–0. doi:10.1016/j.ijsolstr.2018.01.010.

[38] R. Allemang, D. Brown, A correlation coefficient for modal vector analysis., Proceedings of the International Modal Analysis Conference (1982) 110–116.